American Journal of Biochemistry and Biotechnology

Research Paper

Effect of Metal Ions on The Functional Properties of Taro Protein Isolate

Youru Huang, Yingtong Li, Zheng Zhang, Maoqiang Zheng

School of Biotechnology and Food Engineering, Suzhou University of Technology, Changshu, China

Article history
Received: 23 April 2025
Revised: 17 July 2025
Accepted: 5 August 2025

*Corresponding Author:
Maoqiang Zheng, Suzhou University of Technology, Changshu, China
Email: zhengmaoqiang@szut.edu.cn

Abstract: This study investigated the effects of metal ion species and concentrations on the functional properties of taro protein isolate (TPI), extracted from *Colocasia esculenta* corms. The results demonstrated that metal salt solutions could modulate the unfolding and aggregation of TPI, thereby altering its protein-protein and protein-water interactions and significantly affecting the functional properties. When monovalent cation concentration [M^+] was less than or equal to 60 mmol/L or divalent cation concentration [M^{2+}] was below 40 mmol/L, the concentration increasing of metal ions enhanced the solubility of TPI, while reducing the foaming capacity and foam stability, and improving the emulsifying capacity and emulsifying stability. When [M^+] was higher than 60 mmol/L or [M^{2+}] was higher than 40 mmol/L, the solubility of TPI decreased due to partial aggregation, and the foaming capacity and foam stability exhibited antagonistic characteristics, while the emulsifying capacity increased (except for Na^+), and the emulsifying stability decreased. It was worth noting that molecular aggregation involving Ca^{2+} significantly reduced T_{gel} of TPI solution and markedly enhanced the gel strength.

Keywords: Taro protein isolate, Rheological Properties, Foamability, Emulsification

Introduction

Taro (*Colocasia esculenta*), a member of the Araceae family, is characterized by its enlarged underground corms. These corms are relatively low in fat, proteins and vitamins, but are a good source of carbohydrates and minerals. The consumption patterns of taro corms vary among different countries and regions (Himeda et al., 2014; Kaushal et al., 2015). Taro protein isolate (TPI) was extracted from underground corms of taro with a protein content ≥ 90% (Huang et al., 2016). Currently, limited analytical studies were reported on taro protein isolate.

Previous studies demonstrated that taro corms contained diverse protein components. Approximately 11% of the total proteins in taro were identified as albumin, which was rich in essential amino acids such as phenylalanine and leucine (Maga, 1992). Monte-Neshich et al. (1995) characterized globulins in taro corms, which accounted for 80% of the total soluble proteins. Additionally, de Castro et al. (1992), Monte-Neshich et al. (1995), and Pereira et al. (2018) identified a storage protein family termed Tarin, with a relative molecular mass of 12.5 kDa, constituting approximately 40% of the soluble proteins in taro corms. Jiang and Ramsden (1999) demonstrated that taro mucilage contained 93.2-98.2% arabinogalactan-protein (AGP glycoprotein), which exhibited antioxidant activity (Nguimbou et al., 2014). The protein moiety of AGP was primarily composed of aspartic acid/asparagine and glutamic acid/glutamine (Njintang et al., 2011), along with lysine, tryptophan, cysteine, isoleucine, and leucine (Andrade et al., 2015). Notably, lysine, tryptophan, isoleucine, and leucine were classified as essential amino acids (Day, 2013; Cheung et al., 2024). It was proposed that AGP glycoproteins present in taro mucilage served as key components responsible for its emulsifying properties during taro product processing (Andrade et al., 2015,

2020). Huang et al. (2016) prepared TPI by alkali-solubilization and acid-precipitation method and investigated its physicochemical properties, including isoelectric point, denaturation temperature, amino acid composition, and distribution of subunit relative molecular mass.

Although numerous studies on taro proteins have been reported, investigations into their functional properties remained limited. No studies have been published regarding the effects of metal ions on the properties, structure, and functionality of taro protein. This study mainly investigates the effects of four metal ions on the functional properties of TPI, including its rheological behavior, solubility, foaming capacity, and emulsifying characteristics. The research will help us gain a deeper understanding of taro and enrich the variety of taro-based food products.

Materials and Methods

Materials and Chemicals

Taro was purchased from a local market in Changshu, Jiangsu Province, China. All chemical reagents were of analytical grade. Sodium chloride, potassium chloride, sodium hydroxide, and hydrochloric acid were supplied by Jiangsu Qiangsheng Chemical Co., Ltd. Anhydrous calcium chloride, Magnesium chloride were obtained from Shanghai Epichem Reagent Co., Ltd.

Extraction of Taro protein isolate

Taro was peeled and homogenized into a slurry with six volumes of water at 25 °C. The pH of the slurry was adjusted to 8.0, followed by stirring for 30 min to extract protein. Then the slurry was centrifuged at 4000 × g for 15 min using the centrifuge (LXY-II, Medical Analytical, Shanghai), and the supernatant was collected. The supernatant was adjusted to pH 5.0, followed by another centrifugation at 4000 × g for 30 min. The precipitate was collected and the pH was readjusted to 7.0. Finally, the precipitate was freeze-dried (Freezone-6L, LABCONCO, USA) to obtain taro protein isolate. Three sample were prepared and the average protein content measured by the Kjeldahl method was 92.4±0.11% (Quintero et al., 2022).

Rheological Properties

The freeze-dried TPI powder was reconstituted into 8% (w/v) protein solutions using saline solutions (0, 40, 80, and 120 mmol/L) containing KCl, NaCl, $MgCl_2$, and $CaCl_2$ respectively. The rheological properties were analyzed using a Physica rheometer (MCR301, Anton Paar, Austria) equipped with a 50-mm parallel plate radius, a 1-mm gap, and 0.9 mL sample, with silicone oil sealing. The temperature of the base plate was set to 25 °C before adding the sample.

Structure Recovery: Structure recovery of TPI solutions were evaluated using the Hysteresis Area: up-hold-down ramp mode. The experimental parameters were set as follows: the temperature was maintained at 25 °C, the shear rate varied from 0.1 to 200 s^{-1}, held at 200 s^{-1} for 1 min, then decreased from 200 to 0.1 s^{-1}. This protocol was designed to investigate the effects of shear rate on viscosity and structural integrity of TPI solutions.

Frequency Sweep: Frequency sweep tests were conducted at a constant temperature of 25 °C. The rheometer was operated in auto-stress mode with an initial stress of 0.8 Pa and a target strain of 0.5%. The scanning frequency range was performed from 0.5 and 100 s^{-1}. This procedure was used to assess viscoelastic properties of TPI solutions over a wide range of frequencies.

Temperature Sweep: The temperature sweep tests were conducted at a constant angular frequency of 10 rad/s and 0.5% strain. The temperature program involved heating the sample from 25 °C to 95 °C at a rate of 10 °C/min, holding at 95 °C for 1 min, then cooling back to 25 °C at the same rate. This protocol was designed to examine thermal stability and structural changes of TPI solutions over a broad temperature range (Mu et al., 2019).

Solubility

TPI solutions (2.0 mg/mL) were prepared respectively using saline solutions containing KCl, NaCl, $MgCl_2$, and $CaCl_2$ at concentrations of 0, 20, 40, 60, 80, 100, and 120 mmol/L at room temperature of approximately 20 °C. The corresponding salt solutions were used as controls. After centrifugation (3000 × g) for 10 min, the protein content in the supernatant was determined by the Coomassie Brilliant Blue method using a UV-Vis spectrophotometer (UV1800, MAPADA, Shanghai). Solubility of TPI was calculated as follows (Drozłowska et al., 2020):

$$\text{S}\ (\%) = \frac{C_1}{C_0} \times 100 \quad (1)$$

Where, S was the solubility of TPI (%), C_0, C_1 were the protein content (mg/mL) in initial solution and supernatant, respectively

Foaming capacity and Foam Stability

The aforementioned solutions (25 mL each) were homogenized using a high-shear homogenizer (FA25, Fluke Fluid, Shanghai) at 10 000 r/min for 2 min at room temperature. Foam volumes were recorded immediately and 30 min after homogenization (Cano-Medina et al., 2011; Chao and Aluko, 2018). Foaming capacity and foam stability were calculated as follows:

$$FC\ (\%) = \frac{V_0}{25} \times 100 \quad (2)$$

$$FS\ (\%) = \frac{V_{30}}{V_0} \times 100 \quad (3)$$

Where, FC was the foaming capacity (%), FS was the foam stability (%), V_0, V_{30} were the foam volumes (mL) after 0 min and 30 min of homogenization respectively.

Emulsifying capacity and Emulsion Stability

First-grade soybean oil (12.5 mL each) was added to the aforementioned solutions and homogenized at 10 000 r/min for 2 min at room temperature. The emulsion samples were centrifuged at 3 000 r/min for 2 min. Initial heights of emulsion layer and total heights of liquid in the tubes were recorded after homogenization. Then the emulsion samples were incubated at 80 °C for 30 min in a water bath, cooled to room temperature, and centrifuged at 3 000 r/min for 2 min. Final heights of emulsion layer in the tubes were recorded after homogenization (Cano-Medina et al., 2011). Emulsifying capacity and emulsion stability were calculated as follows:

$$EC\ (\%) = \frac{H_i}{H_t} \times 100 \quad (4)$$

$$ES\ (\%) = \frac{H_f}{H_i} \times 100 \quad (5)$$

Where, EC was the emulsifying capacity (%), ES was the emulsion stability (mL), H_i was the initial height (cm) of emulsion layer in the tubes, H_t was total height (cm) of liquid in the tubes, H_f was the height (cm) of emulsion layer after incubation and centrifugation.

Data Processing

All experiments were conducted in triplicate, with results expressed as mean ± standard deviation. Data were analyzed by one-way ANOVA, followed by Tukey's post hoc test (Origin 2024, OriginLab Corporation, Northampton, MA, USA).

Results and Discussion

Rheological Properties of Taro protein isolate

The influence of shear rate on viscosity of TPI solutions with different salt species and concentrations was shown in Figure (1) With increasing shear rate, the viscosity of TPI solutions exhibited rapid decline across all tested metal ion concentrations. When the shear rate reached a certain value, their effects on viscosity became minimal, which was indicative of shear-thinning behavior (Schreuders et al., 2021). It was a common characteristic of most food protein solutions, primarily due to the oriented alignment of protein molecules as the shear rate increases (Mu et al., 2019). The viscosity at a shear rate of 0 s^{-1} was referred to as the apparent initial viscosity. Compared with the control sample, the apparent initial viscosities of the TPI solutions with added metal ions showed a significant decrease. The order of reduction magnitude was $Ca^{2+} > Na^{+} > Mg^{2+} > K^{+}$. When the external force was removed, the viscosities of all TPI samples could not fully recover, exhibiting a weak hysteresis phenomenon. At an ionic concentration of 80 mmol/L, the hysteresis loop area and onset point reached their minimum values for all samples. The observed hysteresis loops were ascribed to the inability of the aligned protein molecules to instantaneously recover their original conformation upon the removal of shear stress.

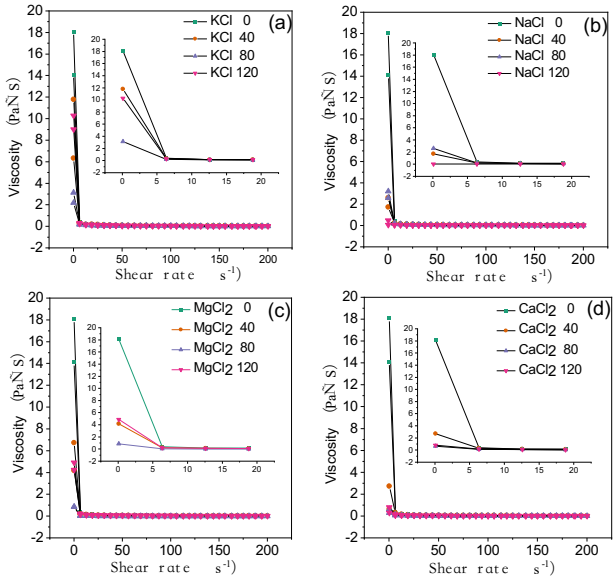

Fig. 1. The influence of shear rate on viscosity of TPI solutions with different salt species (a, KCl; b, NaCl; c, $MgCl_2$; d, $CaCl_2$) and concentrations (0, 40, 80, 120 mmol/L)

The results revealed that neutral salts significantly modulated the solubility and aggregation behavior of TPI in aqueous solutions. At low ionic strengths (<80 mmol/L), TPI demonstrated improved solubility and maintained relatively stable conformational structures due to the salting-in effect, which consequently decreased the apparent initial viscosity and diminished hysteresis responses. However, when the salt concentration exceeded 80 mmol/L, the salting-out effect induced partial protein aggregation, leading to a marked increase in apparent initial viscosity and hysteresis loops.

Figure (2) depicted the angular frequency sweeps of storage (G') and loss (G") moduli for the 8% (w/v) TPI solutions with different salt species and concentrations. In the angular frequency range of 0.5-10 s^{-1}, G' and G" of different metal ion concentrations exhibited parallel trends, with the exception of 80 mmol/L [Mg^{2+}] and

DOI:10.3844/ajbbsp.2025.362.372

120 mmol/L [Ca^{2+}] systems where modulus crossover was observed at 5 s^{-1} and 4.55 s^{-1}, respectively. Subsequent solubility analysis revealed that the minimum solubility of TPI occurred at 120 mmol/L [Ca^{2+}], whereas the maximum solubility was achieved at 40 mmol/L [Mg^{2+}]. Notably, a marked salting-out effect became evident when [Mg^{2+}] reached 80 mmol/L as follows Table (3).

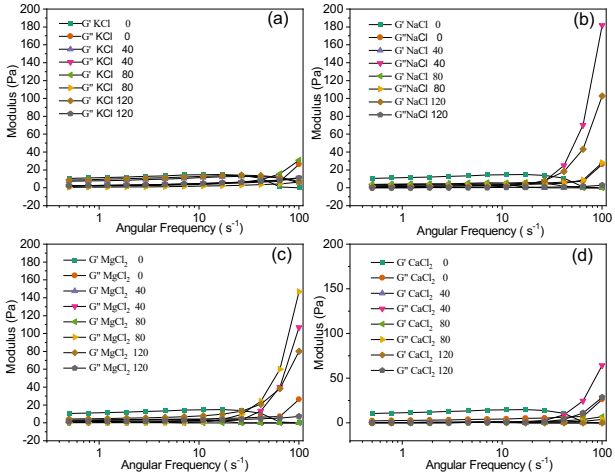

Fig. 2. Frequency scanning curves of TPI solutions with different salt species (a, KCl; b, NaCl; c, $MgCl_2$; d, $CaCl_2$) and concentrations (0, 40, 80, 120 mmol/L)

According to the pioneering work of Winter and Chambon (1986), the gelation point was characterized by identical power-law exponents for both G' and G" over a broad frequency range (i.e., G'~G"~$\omega^{1/2}$). This implied parallel frequency dependence of G' and G" with a frequency-independent phase angle at the gelation point, which had been established as a fundamental criterion for identifying the onset of gel formation. Notably, the convergence of G' and G" into parallel trajectories marked the critical sol-gel transition where protein solutions transformed from viscous fluids to elastic networks (Schreuders et al., 2021). As demonstrated in Figure (2), 8% TPI solutions successfully formed gels upon cooling after heating, a finding further corroborated by subsequent temperature-sweep rheological measurements.

The ratio G"/G', defined as the loss tangent (tanδ), served as a key indicator of viscoelastic characteristics. Higher tanδ values (tanδ > 1) reflected dominant viscous behavior with pseudo-fluid properties, whereas lower values (tanδ < 1) indicated predominant elastic behavior with pseudo-solid properties. Comparative analysis at an angular frequency of 4.55 s^{-1} revealed that tanδ reached minimum values at 80 mmol/L for Na^+ and Ca^{2+}, and 120 mmol/L for K^+ and Mg^{2+}. This minimum tanδ coincided with metal ion-induced protein aggregation that significantly enhanced the elastic component of the system. These findings demonstrated that salting-in effect at low ion concentrations and salting-out effect at high concentrations critically influenced TPI solubility, consequently modulating its gelling properties. Notably, excessive protein aggregation was found to impair gelation performance, as evidenced by deteriorated parallelism between G' and G" and eventual modulus crossover. Therefore, controlling protein aggregation was identified as the determining factor during the development of gel-type taro protein products.

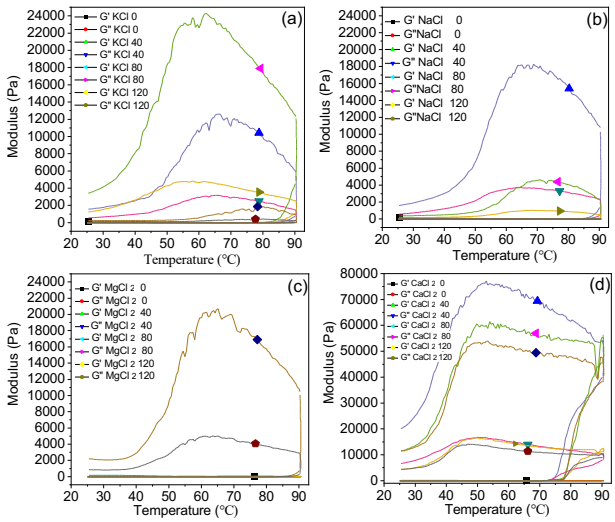

Fig. 3. Temperature-sweep curves of the TPI solutions with different salt species (a, KCl; b, NaCl; c, $MgCl_2$; d, $CaCl_2$) and concentrations (0, 40, 80, 120 mmol/L)

Figure (3) presented the temperature sweeps of the storage (G') and loss (G") moduli for the 8% (w/v) TPI solutions with different salt species and concentrations. The G' and G" values of the TPI in $CaCl_2$ were significantly higher than those of the other three solutions, so the range of the chart's vertical axis was increased to 80,000 Pa. Based on the methodology established by Li et al. (2006), the gelation temperature (T_{gel}) was operationally defined as the temperature at which G' exhibited rapid deviation from baseline. As summarized in Table (1), the measured T_{gel} values demonstrated significant variations depending on both metal ion species and their concentrations. For a given metal ion species, significant concentration-dependent effects on T_{gel} were observed, with the exception of [Mg^{2+}] at 40 and 120 mmol/L which exhibited identical gelation temperature modulation. Notably, the addition of K^+ at 80 mmol/L reduced T_{gel} by 19.4°C compared to the control. The most pronounced effects were observed for Ca^{2+}, where incremental concentration

increases led to T_{gel} reductions of 24.5 °C, 17.3 °C, and 32.9 °C, respectively. While plant proteins from different sources often displayed divergent material properties, the observed trend of Calcium-induced gelation temperature depression has been consistently reported across various plant protein systems, including soy protein isolates (Zhao et al., 2016). At the concentration of 40 mmol/L, only Ca^{2+} demonstrated significantly distinct effects on T_{gel} compared to the other three metal ions. When the concentration reached 80 mmol/L, K^+ and Ca^{2+} exhibited similar modulation patterns on T_{gel} to Na^+ and Mg^{2+}, respectively. However, despite sharing the same valence states, K^+/Na^+ and Ca^{2+}/Mg^{2+} pairs showed markedly different impacts on gelation temperature. At the highest tested concentration (120 mmol/L), all metal ions displayed statistically significant differences in their T_{gel} modulation effects.

Table 1. Gelation temperature (°C) of TPI solutions during the temperature-programmed heating process with different salt species (KCl, NaCl, $MgCl_2$, $CaCl_2$) and concentrations (Conc., 0, 40, 80, 120 mmol/L)

Conc. (mmol/L)	KC1	NaC1	$MgCl_2$	$CaC1_2$
0	78.2 ± 0.8^{aA}	78.2 ± 0.8^{aA}	78.2 ± 0.8^{aA}	78.2 ± 0.8^{aA}
40	75.3 ± 0.7^{aB}	74.7 ± 0.9^{aB}	75.8 ± 0.6^{aB}	53.7 ± 0.3^{bB}
80	58.8 ± 0.3^{aC}	80.8 ± 0.6^{bC}	81.4 ± 1.1^{bC}	60.9 ± 0.5^{aC}
120	79.8 ± 0.5^{aD}	82.9 ± 1.3^{bD}	75.8 ± 0.5^{cB}	45.3 ± 0.6^{dD}

Note: Different letters indicate significant ($P < 0.05$) differences, lowercase letters between salt species and capital letters between metal ion concentrations.

G' was denoted as the storage modulus, also referred to as the elastic modulus, which represented the gel strength. Table (2) recorded the storage modulus (G') at key temperature points during the complete thermal scanning cycle of TPI solutions, which underwent heating from 25 °C through the denaturation temperature (71.3±0.2 °C) to 90 °C followed by cooling back to 25 °C (Huang et al., 2016). At the initial temperature, the addition of metal ions significantly reduced G' of TPI solutions compared to the control. This trend persisted at the denaturation temperature for K^+, Na^+, and Mg^{2+}, whereas Ca^{2+} exhibited a distinct behavior by markedly increasing G'. Although protein denaturation and unfolding occurred at this stage, intermolecular interactions (electrostatic and hydrophobic aggregation) remained incomplete until reaching 90 °C, where all metal ions exerted maximal effects on G'. Notably, Ca^{2+} induced the most dramatic enhancement, elevating G' by several thousand-fold relative to the initial value, resulting in irreversible pre-gel formation. Upon cooling to 25 °C, stable protein gels formed through non-covalent interactions (e.g., hydrophobic forces and hydrogen bonds) between protein-protein and protein-ion complexes (Chu et al., 2019; Himeda et al., 2014). Comparative analysis revealed that Ca^{2+} exerted the strongest influence on G', followed by K^+ and Na^+, while Mg^{2+} showed minimal effects at 40 and 80 mmol/L. These findings demonstrate that metal ion concentration critically modulates both denaturation and aggregation behaviors of taro protein isolate.

Compared with other metal ions, Ca^{2+} exhibited a remarkably prominent contribution to G' throughout the entire process from TPI denaturation to gel formation. The primary reason was that Ca^{2+} could form bridges between negatively charged amino acid residues of adjacent polypeptides (Chu et al., 2019), thereby strengthening the gel structure. However, excessive Ca^{2+} induced protein aggregation via calcium bridging, leading to clot formation, reduced gel homogeneity, and consequently, fluctuations in the measured storage modulus.

Solubility of Taro protein isolate

Solubility served as a prerequisite for the functional properties of proteins, as insoluble proteins exhibited severely limited applications in food systems. The low solubility of most plant protein ingredients was identified as a major obstacle to fully replacing dairy proteins for stabilizing colloidal food systems (Hinderink et al., 2021; Khalid et al., 2003). During food processing (e.g., exposure to strong acids/bases, thermal treatment, or neutral salts), structural modifications of food proteins could occur, leading to the formation of protein aggregates and a consequent increase in insoluble protein content.

As shown in Table (3), monovalent metal ions (M^+) demonstrated a concentration-dependent effect on protein solubility. Within the range of 0-60 mmol/L, increasing ionic strength consistently enhanced protein solubility. However, when the concentration exceeded 60 mmol/L, further elevation of M^+ concentration resulted in a significant decline in solubility (Mu et al., 2019). At low salt concentrations, larger positively charged metal ions penetrated between suspended TPI particles bearing similar negative charges, displacing the originally associated water molecules and

facilitating protein dispersion into the aqueous phase. However, when the salt concentration exceeded a critical threshold (60 mmol/L), the solubility of TPI displayed a marked decline with further increases in ionic strength. This reversal was primarily attributed to the dehydration of hydrophobic domains on the protein surface. At high salt concentrations, the water molecules originally clustered around these hydrophobic regions were extracted to hydrate the ions, thereby exposing the nonpolar residues. The subsequent intermolecular hydrophobic interactions promoted protein aggregation and precipitation, ultimately leading to decreased solubility (Hinderink et al., 2021).

Table 3. Solubility (%) of TPI in aqueous solutions with different salt species (KCl, NaCl, $MgCl_2$, $CaCl_2$) and concentrations (0, 20, 40, 60, 80, 100, 120 mmol/L)

Conc. (mmol/L)	KCl	NaCl	$MgCl_2$	$CaCl_2$
0	69.03 ± 0.76^{aA}	69.03 ± 0.76^{aA}	69.03 ± 0.76^{aA}	69.03 ± 0.76^{aA}
20	70.03 ± 1.03^{aA}	81.30 ± 1.07^{bB}	73.91 ± 0.91^{cB}	72.90 ± 0.74^{cB}
40	71.76 ± 0.76^{aB}	81.10 ± 0.94^{bB}	74.56 ± 1.04^{cB}	75.09 ± 0.80^{cC}
60	77.18 ± 0.89^{aC}	84.10 ± 0.88^{bC}	72.21 ± 0.87^{cC}	69.19 ± 1.03^{dA}
80	72.28 ± 1.04^{aB}	80.60 ± 0.98^{bB}	71.77 ± 1.04^{aC}	61.43 ± 0.85^{cD}
100	72.04 ± 0.90^{aB}	79.20 ± 1.08^{bD}	67.94 ± 0.93^{cA}	61.49 ± 0.83^{dD}
120	71.10 ± 1.06^{aB}	77.10 ± 0.81^{bE}	62.31 ± 0.83^{cD}	60.01 ± 0.80^{dE}

Note: Different letters indicate significant ($P < 0.05$) differences, lowercase letters between salt species and capital letters between metal ion concentrations.

In contrast, divalent metal ions (M^{2+}) exhibited distinct behavior. Within the concentration range of 0-40 mmol/L, M^{2+} effectively enhanced protein solubility. However, when the concentration exceeded 40 mmol/L, further addition of M^{2+} resulted in a marked decrease in solubility. The reduced solubility could be explained by the higher charge density and larger atomic radius characteristic of divalent ions relative to monovalent ions.

Foaming Capacity and Foam Stability of Taro protein isolate

Foaming capacity, as one of the functional properties of proteins, was influenced by multiple factors including pH, ionic strength, and salt species (Bučko et al., 2018; Chao and Aluko, 2018). Table (4) presents the effects of different metal ions and their concentrations on the foaming capacity and foam stability of taro protein isolate solutions. Compared to the control, the addition of metal ions significantly reduced both the foaming capacity and foam stability in TPI solutions. The extent of reduction in foaming capacity followed the order: $Mg^{2+} > Ca^{2+} > K^+ > Na^+$, while the decrease in foam stability exhibited the trend: $Ca^{2+} > Mg^{2+} > K^+ > Na^+$. Foam stability is generally positively correlated with solution viscosity. Higher viscosity retarded the drainage of thin liquid films between bubbles, thereby enhancing foam stability (Hu et al., 2018). The observed decline in foam stability of metal ion-treated TPI solutions was consistent with the reduction in apparent initial viscosity.

The critical concentration threshold of monovalent metal ions (M^+) affecting the foaming properties of TPI was identified between 60 and 80 mmol/L. When [M^+] was equal to or below 60 mmol/L, both foaming capacity and foam stability of TPI showed a progressive decrease with increasing [M^+]. At [M^+] exceeding 60 mmol/L, the effects of [M^+] demonstrated antagonistic characteristics where increasing [Na^+] led to reduced foaming capacity but enhanced foam stability, while elevated [K^+] resulted in improved foaming capacity but diminished foam stability.

In comparison, divalent metal ions (M^{2+}) exhibited a lower critical concentration threshold ranging from 20 to 40 mmol/L for influencing foaming performance. This finding was potentially associated with the bridging interactions between M^{2+} and carboxyl groups of protein subunits (Chu et al., 2019). Below 40 mmol/L, both foaming capacity and foam stability decreased with increasing [M^{2+}]. At [M^{2+}] of 40 mmol/L or higher, similar antagonistic effects were observed where higher [M^{2+}] decreased foaming capacity while simultaneously improving foam stability.

The unique foaming behavior of TPI was presumably associated with its charge characteristics. Previous work from our laboratory (Huang et al., 2016) had determined the isoelectric point (pI) of TPI to be 5.0. For this study, TPI was prepared by alkaline extraction and acid precipitation, with the final pH

adjusted to 7.0 before freeze-drying. All investigations into the effects of metal ion species and concentrations on functional properties including rheological and interfacial characteristics were performed using deionized water. At near-neutral pH conditions (above the pI of TPI), the protein molecules carried net negative charges and experienced mutual electrostatic repulsion. In metal ion concentrations up to 60 mmol/L for [M^+] and 40 mmol/L for [M^{2+}], TPI maintained high solubility with extended polypeptide chains and increased molecular flexibility. This conformation promoted exposure of hydrophobic domains, facilitating their adsorption and structural rearrangement at interfaces, which accounted for the observed superior foaming performance. However, when metal ion concentrations surpassed 60 mmol/L for [M^+] or 40 mmol/L for [M^{2+}], partial protein aggregation occurred with concomitant solubility reduction. This transition led to the characteristic antagonistic relationship between foaming capacity and foam stability (Cano-Medina et al., 2011).

Emulsifying Capacity and Emulsion Stability of Taro protein isolate

The effects of four metal ions at varying concentrations on emulsifying capacity and emulsion stability of TPI solutions were presented in Table (5). Overall, compared with the control sample, the addition of metal ions significantly enhanced both emulsifying capacity and emulsion stability of TPI solutions. The improvement in the emulsifying capacity followed the order: $Ca^{2+} > Mg^{2+} > K^+ > Na^+$, whereas the enhancement in the emulsion stability exhibited the trend: $Ca^{2+} > Na^+ > Mg^{2+} > K^+$.

At lower metal ion concentrations, the emulsifying capacity and emulsion stability of TPI increased with rising concentrations of both M^+ and M^{2+}, except for Na^+, which exhibited a minimal effect on the emulsifying capacity (Zhu et al., 2017). The critical threshold for [M^+] was observed at 60-80 mmol/L. When [M^+] exceeded 60 mmol/L, the emulsion stability of TPI decreased. However, Na^+ and K^+ exerted opposite effects on emulsifying capacity. For M^{2+}, the critical concentration range was 40-60 mmol/L. Above 40 mmol/L, the emulsion stability of TPI declined, whereas emulsifying capacity continued to show a gradual increasing trend.

The emulsification properties of protein solutions exhibited a certain correlation with their solubility (Cano-Medina et al., 2011; Chao and Aluko, 2018). The effects of the four metal ions and their concentrations on emulsifying capacity and emulsion stability of TPI solutions were largely consistent with their impacts on solubility. Under low salt concentrations, the solubility of TPI increased with rising salt levels, leading to enhanced protein adsorption at the oil-water interface. This promoted protein-protein interactions and the formation of a robust interfacial film (Chao and Aluko, 2018), thereby improving emulsification performance, including both emulsifying capacity and emulsion stability.

Upon exceeding a critical salt concentration, the solubility of TPI decreased. Water molecules surrounding hydrophobic regions on the protein surface were withdrawn and hydrated by salt ions, exposing hydrophobic domains that preferentially migrated to the oil-water interface (Andrade et al., 2020). Concurrently, protein unfolding occurred, enhancing emulsifying capacity. Given that the denaturation temperature of TPI was 71.3±0.2 °C, subsequent stability testing at 80 °C (above denaturation threshold) induced aggregation of the already adsorbed, unfolded proteins at the interface. This process reduced the elasticity of the interfacial film and impaired its capacity to stabilize O/W emulsions, ultimately leading to emulsion breakdown and decreased emulsion stability (Chao and Aluko, 2018). An analogous phenomenon was observed during heat-induced formation of soy protein nanoparticle aggregates. Compared to low ionic strength conditions, aggregates formed at higher ionic strength exhibited larger particle sizes and elevated surface hydrophobicity, resulting in diminished emulsifying capacity (Zhu et al., 2017). Cui et al. (2014) similarly reported differential adsorption behaviors between aggregated and non-aggregated fractions of heated soy proteins when studying NaCl concentration effects on emulsification properties and interfacial adsorption.

Conclusions

Consistent with most food protein solutions, TPI solutions exhibited shear-thinning behavior, characteristic of pseudoplastic fluids. Frequency sweep tests revealed that both the species and concentration of metal ions significantly influenced the solubility and aggregation state of TPI, consequently affecting its gelling properties. During programmed heating, the metal ion concentration in the solution markedly impacted the denaturation and aggregation behavior of TPI. Among all tested metal ions, [Ca^{2+}] demonstrated the most pronounced effects throughout the entire process from protein denaturation to gel network formation. Increasing [Ca^{2+}] led to a substantial

decrease in T_{gel} and a rapid enhancement of G'.

At $[M^+]$ ranging from 0 to 60 mmol/L, TPI solubility increased with rising ionic strength. However, when $[M^+]$ exceeded 60 mmol/L, further increases led to a progressive decline in protein solubility. In contrast, M^{2+} exhibited distinct behavior. Within $[M^{2+}]$ range of 0-40 mmol/L, M^{2+} enhanced TPI solubility, whereas beyond this threshold (40 mmol/L), additional M^{2+} resulted in reduced solubility.

Foaming capacity and foam stability of TPI decreased progressively with increasing metal ion concentrations at $[M^+]$ up to 60 mmol/L or $[M^{2+}]$ below 40 mmol/L. Beyond these critical concentrations ($[M^+]$ above 60 mmol/L or $[M^{2+}]$ at 40 mmol/L and higher), the system displayed an apparent antagonistic effect: while partial protein aggregation led to reduced solubility, this was accompanied by unexpected improvements in both foaming capacity and stability.

At relatively low salt concentrations, the solubility of TPI increased progressively with rising salt concentration, leading to enhanced protein adsorption at the oil-water interface and consequently improved emulsifying capacity and emulsion stability. Upon exceeding critical salt concentrations ($[M^+]$ above 60 mmol/L or $[M^{2+}]$ beyond 40 mmol/L), TPI solubility declined significantly.

As a novel plant-based protein, TPI demonstrates promising application potential in ice cream, meat analogues, sauce thickening, and specialized dietary products due to its unique functional properties. Controlling the effects of salt ions and preventing taro protein isolate aggregation will facilitate the optimization of processing techniques for gel-type product and enhance the gel product quality.

Table 2. Storage modulus （Pa） of taro protein isolate solution at key temperatures points during heating with different salt species (KCl, NaCl, $MgCl_2$, $CaCl_2$) and concentrations (0, 40, 80, 120 mmol/L)

Key points	Conc. (mmol/L)	KCl	NaCl	$MgCl_2$	$CaCl_2$
25℃ （Initial temperature）	0	16.1 ± 0.5^{aA}	16.1 ± 0.5^{aA}	16.1 ± 0.5^{aA}	16.1 ± 0.5^{aA}
	40	11.8 ± 0.4^{aB}	6.5 ± 0.2^{bB}	5.1 ± 0.2^{bB}	2.9 ± 0.1^{cB}
	80	4.1 ± 0.1^{aC}	7.1 ± 0.3^{bB}	1.9 ± 0.1^{cC}	0.0 ± 0.0^{cC}
	120	14.4 ± 0.5^{aD}	0.7 ± 0.0^{bC}	8.8 ± 0.3^{cD}	1.7 ± 0.1^{bC}
71.3±0.2℃ （ Denaturation temperature）	0	7.4 ± 0.3^{aA}	7.4 ± 0.3^{aA}	7.4 ± 0.2^{aA}	7.4 ± 0.3^{aA}
	40	7.6 ± 0.3^{aA}	5.8 ± 0.1^{aA}	2.3 ± 0.1^{bB}	56.3 ± 1.7^{cB}
	80	6.1 ± 0.2^{aA}	3.2 ± 0.1^{bB}	1.2 ± 0.0^{cB}	41.5 ± 1.3^{dC}
	120	3.8 ± 0.1^{aB}	0.1 ± 0.0^{bC}	3.6 ± 0.1^{aC}	72.3 ± 2.1^{cD}
90℃ (Maximum temperature)	0	32.2 ± 1.6^{aA}	32.2 ± 1.6^{aA}	32.2 ± 1.6^{aA}	32.2 ± 1.6^{aA}
	40	6080.0 ± 194.6^{aB}	11000.0 ± 342.0^{bB}	47.2 ± 1.5^{cB}	54200.0 ± 1134.0^{dB}
	80	12500.0 ± 412.0^{aC}	2320.0 ± 73.2^{bC}	4.3 ± 0.1^{cC}	55500.0 ± 1021.0^{dC}
	120	922.0 ± 29.5^{aD}	0.5 ± 0.0^{bD}	10900.0 ± 341.3^{cD}	47500.0 ± 1205.0^{dD}
25℃ （Final temperature）	0	175.0 ± 5.3^{aA}	175.0 ± 5.3^{aA}	175.0 ± 5.3^{aA}	175.0 ± 5.3^{aA}
	40	1570.0 ± 47.1^{aB}	1620.0 ± 45.6^{aB}	54.6 ± 1.3^{bB}	20100.0 ± 503.0^{cB}
	80	3430.0 ± 102.1^{aC}	378.0 ± 11.3^{bC}	24.4 ± 0.7^{cC}	11500.0 ± 145.0^{dC}
	120	248.0 ± 7.1^{aD}	8.0 ± 0.2^{bD}	2240.0 ± 66.2^{cD}	11600.0 ± 108.0^{dD}

Note: Different letters indicate significant ($P < 0.05$) differences, lowercase letters between salt species and capital letters between metal ion concentrations.

Table 4. Foaming capacity (%) and foam stability (%) of TPI in aqueous solutions with different salt species (KCl, NaCl, $MgCl_2$, $CaCl_2$) and concentrations (0, 20, 40, 60, 80, 100, 120 mmol/L)

Conc. (mmol/L)	FC (%)				FS (%)			
	KCl	NaCl	$MgCl_2$	$CaCl_2$	KCl	NaCl	$MgCl_2$	$CaCl_2$
0	46.30±1.36 aA	46.30±1.36 aA	46.30±1.36 aA	46.30±1.36 aA	81.84±1.87 aA	81.84±1.87 aA	81.84±1.87 aA	81.84±1.87 aA
20	30.59±0.87 aB	41.81±1.20 bB	24.57±0.69 cB	15.66±0.34 dB	79.14±1.72 aB	79.49±2.36 aB	73.95±2.00 bB	66.92±1.77 cB
40	26.19±0.69 aC	30.43±0.67 bC	37.50±0.92 cC	51.77±1.48 dC	77.27±1.65 aC	80.77±1.82 bA	27.09±0.56 cC	25.00±0.54 dC
60	19.67±0.48 aD	29.21±0.85 bC	33.72±0.76 cD	40.23±0.96 dD	14.81±0.34 aD	49.35±1.03 bC	31.03±0.92 cD	25.71±0.70 dC
80	36.26±0.75 aE	53.42±1.37 bD	33.52±0.94 cD	39.52±0.93 dD	54.84±1.44 aE	69.23±1.91 bD	35.67±0.83 cE	30.99±0.84 dD
100	52.38±1.42 aF	48.33±1.27 bE	35.88±0.93 cE	35.23±0.83 cE	50.00±1.10 aF	77.95±1.59 bE	62.30±1.76 cF	41.94±1.18 dE
120	59.26±1.59 aG	45.41±1.12 bA	40.11±1.04 cF	41.63±0.88 dF	49.75±1.03 aF	79.88±1.88 bB	65.35±1.72 cG	45.28±1.34 dF

Note: Different letters indicate significant ($P < 0.05$) differences, lowercase letters between salt species and capital letters between metal ion concentrations.

Table 5. Emulsifying capacity (%) and Emulsion stability (%) of TPI in aqueous solutions with different salt species (KCl, NaCl, $MgCl_2$, $CaCl_2$) and concentrations (0, 20, 40, 60, 80, 100, 120 mmol/L)

Conc. (mmol/L)	EC (%)				ES (%)			
	KCl	NaCl	$MgCl_2$	$CaCl_2$	KCl	NaCl	$MgCl_2$	$CaCl_2$
0	13.70±0.31 aA	13.70±0.31 aA	13.70±0.31 aA	13.70±0.31 aA	55.31±1.07 aA	55.31±1.07 aA	55.31±1.07 aA	55.31±1.07 aA
20	32.33±1.75 aB	31.82±1.49 aB	22.21±0.57 bB	15.12±0.37 cB	57.83±1.06 aB	69.49±1.31 bB	69.50±1.19 bB	74.51±1.46 cB
40	36.42±2.11 aC	30.43±1.82 bC	71.24±1.98 cC	74.91±1.77 dC	64.69±0.98 aC	80.77±1.40 bC	87.25±1.52 cC	87.94±1.32 cC
60	42.54±2.19 aD	29.21±1.62 bD	70.22±1.96 cD	80.83±1.69 dD	72.00±1.23 aD	89.35±1.48 bD	76.67±1.20 cD	81.23±1.18 dD
80	64.91±2.63 aE	73.44±3.09 bE	80.51±2.02 cE	79.71±1.76 cE	70.28±1.37 aE	69.23±0.95 bB	68.00±0.97 cE	73.55±1.14 dE
100	43.82±2.09 aF	28.31±1.42 bD	72.63±1.83 cF	82.64±2.39 dF	61.50±0.95 aF	67.95±1.23 bE	59.69±1.02 cF	70.31±1.06 dF
120	44.11±2.43 aF	27.52±1.39 bD	73.31±1.81 cF	76.42±2.19 dG	49.01±0.69 aG	51.34±0.73 bF	55.61±0.75 cA	62.50±0.84 dG

Note: Different letters indicate significant ($P < 0.05$) differences, lowercase letters between salt species and capital letters between metal ion concentrations.

Acknowledgements

This study was supported by the Suzhou University of Technology.

Funding Information

This study was sponsored by the Research Start-up Funding of Suzhou University of Technology (No. KYZ2020043Q)

Author's Contributions

Youru Huang: Project administration, Conceptualization, Writing - Original Draft.
Yingtong Li: Investigation, Methodology, Resources.
Zheng Zhang: Software, Formal Analysis, Visualization.
Maoqiang Zheng: Funding Acquisition, Supervision, Validation, Data Curation, Writing - Review & Editing.

Ethics

This article is an original work and contains unpublished material. All authors have read and approved the manuscript, and no ethical violations are involved.

Declarations

The authors declare no competing financial or non-financial interests.

References

Andrade, L. A., Nunes, C. A., & Pereira, J. (2015). Relationship between the chemical components of taro rhizome mucilage and its emulsifying property. *Food Chem*istry, *178*, 331-338. https://doi.org/10.1016/j.foodchem.2015.01.094

Andrade, L. A., Silva, D. A. O., Nunes, C. A., & Pereira, J. (2020). Experimental techniques for the extraction of taro mucilage with enhanced emulsifier properties using chemical characterization. *Food Chemistry*, *327*, 127095. https://doi.org/10.1016/j.foodchem.2020.127095

Bučko, S., Katona, J., Petrovic, L., Milinković, J., Fraj, J., Spasojević, L., & Miller, R. (2018). An investigation on the influence of pH and ionic strength on the adsorption and interfacial dilatational properties at the oil-water interface of pumpkin (Cucurbita pepo) seed protein hydrolysate. *Journal of The Serbian Chemical Society*, *83*(7-8), 847-861. https://doi.org/10.2298/JSC171120042B

Cano-Medina, A., Jiménez-Islas, H., Dendooven, L., Herrera, R. P., González-Alatorre, G., & Escamilla-Silva, E. M. (2011). Emulsifying and foaming capacity and emulsion and foam stability of sesame protein concentrates. *Food Research International*, *44*(3), 684-692. https://doi.org/10.1016/j.foodres.2010.12.015

Chao, D., & Aluko, R. E. (2018). Modification of the structural, emulsifying, and foaming properties of an isolated pea protein by thermal pretreatment. *CyTA - Journal of Food*, *16*(1), 357-366. https://doi.org/10.1080/19476337.2017.1406536

Cheung, S. N., Lieberman, H. R., Pasiakos, S. M., Fulgoni, V. L., & Berryman, C. E. (2024). Associations between Essential Amino Acid Intake and Functional Health Outcomes in Older Adults: Analysis of the National Health and Nutrition Examination Survey, 2001–2018. *Current Developments in Nutrition*, *8*(8), 104411. https://doi.org/10.1016/j.cdnut.2024.104411

Chu, L., Yang, L., Li, J., Lin, L., & Zheng, G. (2019). Effect of Smilax china L. starch on the gel properties and interactions of calcium sulfate-induced soy protein isolate gel. *International Journal of Biological Macromolecules*, *135*, 127-132. https://doi.org/10.1016/j.ijbiomac.2019.05.130

Cui, Z. M., Chen, Y. M., Kong, X. Z., Zhang, C. M., & Hua, Y.F. (2014). Emulsifying Properties and Oil/Water (O/W) Interface Adsorption Behavior of Heated Soy Proteins: Effects of Heating Concentration, Homogenizer Rotating Speed, and Salt Addition Level. *Journal of Agricultural and Food Chemistry*, *62*(7), 1634-1642. https://doi.org/10.1021/jf404464z

Day, L. (2013). Proteins from land plants - Potential resources for human nutrition and food security. *Trends in Food Science & Technology*, *32*(1), 25-42. https://doi.org/10.1016/j.tifs.2013.05.005

de Castro, L. A., Carneiro, M., Neshich, D. de. C, & de Paiva, G. R, (1992). Spatial and temporal gene expression patterns occur during corm development. *Plant Cell, 4*(12), 1549-1559. https://doi.org/10.1105/tpc.4.12.1549

Drozłowska, E., Weronis, M., & Bartkowiak, A. (2020). The influence of thermal hydrolysis process on emulsifying properties of potato protein isolate. *Journal of Food Science and Technology*, *57*(3), 1131-1137. https://doi.org/10.1007/s13197-019-04148-z

Himeda, M., Njintang, Y. N., Gaiani, C., Nguimbou, R. M., Scher, J., Facho, B., & Mbofung, C. M. F. (2014). Physicochemical and thermal properties of taro (*Colocasia esculenta sp*) powders as affected by state of maturity and drying method. *Journal of Food Science and Technology*, *51*(9), 1857-1865. https://doi.org/10.1007/s13197-012-0697-9

Hinderink, E. B. A., Boire, A., Renard, D., Riaublanc, A., Sagis, L. M. C., Schroën, K., Bouhallab, S., Famelart, M., Gagnaire, V., Guyomarc'h, F., & Berton-Carabin, C. C. (2021). Combining plant and dairy proteins in food colloid design. *Current Opinion in Colloid & Interface Science*, *56*, 101507. https://doi.org/10.1016/j.cocis.2021.101507

Hu, G., Zhao, Y., Gao, Q., Wang, X., Zhang, J., Peng, X., Tanokura, M., & Xue, Y. (2018). Functional properties of Chinese yam (Dioscorea opposita Thunb. cv. Baiyu) soluble protein. *Journal of Food Science and Technology*, *55*, 381-388. https://doi.org/10.1007/s13197-017-2948-2

Huang, Y., Wang, J., Zhu, D., Li, X., & Xu, T. (2016). Physicochemical Characterization of Taro Protein Isolates. *Shipin Kexue/Food Science (Chinese)*, *37*(15), 45-48. https://doi.org/10.7506/spkx1002-6630-201615008

Jiang, G., & Ramsden, L. (1999). Characterisation and yield of the arabinogalactan-protein mucilage of taro corms. *Journal of the Science of Food and Agriculture*, *79*(5), 671-674. https://doi.org/10.1002/(SICI)1097-0010(199904)79:5<671::AID-JSFA233>3.0.CO;2-H

Kaushal, P., Kumar, V., & Sharma, H.K. (2015). Utilization of taro (Colocasia esculenta): A review. *Journal of Food Science and Technology*, *52*(1), 27-40. https://doi.org/10.1007/s13197-013-0933-y

Khalid, E. K., Babiker, E.E., Tinay, & A. E. (2003). Solubility and functional properties of sesame seed proteins as influenced by pH and/or salt concentration. *Food Chemistry*, *82*(3), 361-366. https://doi.org/10.1016/S0308-8146(02)00555-1

Li, J., Eleya, M.O., & Gunasekaran, S. (2006). Gelation of whey protein and xanthan mixture: Effect of heating rate on rheological properties. *Food Hydrocolloids*, *20*(5), 678-686. https://doi.org/10.1016/j.foodhyd.2005.07.001

Maga, J. A. (1992). Taro: Composition and food uses. *Food Reviews International*, *8*(3), 443-473. https://doi.org/10.1080/87559129209540948

Monte-Neshich, D. C., Rocha, T. L., Guimarães, R. L., Santana, E. F., Loureiro, M. E., Valle, M., & Grossi, de Sá, M. F. (1995). Characterization and spatial localization of the major globulin families of taro (Colocasia esculenta L. Schott) tubers. *Plant Science*, *112*(2), 149-159. https://doi.org/10.1016/0168-9452(95)04257-1

Mu, B., Xu, H., Li, W., Xu, L., & Yang, Y. (2019). Spinnability and rheological properties of globular soy protein solution. *Food Hydrocolloids*, *90*, 443-451. https://doi.org/10.1016/j.foodhyd.2018.12.049

Nguimbou, R. M., Boudjeko, T., Njintang, N. Y., Himeda, M., Scher, J., & Mbofung, C. M. F. (2014). Mucilage chemical profile and antioxidant properties of giant swamp taro tubers. *Journal of Food Science and Technology*, *51*(12), 3559-3567. https://doi.org/10.1007/s13197-012-0906-6

Njintang, N. Y., Boudjeko, T., Tatsadjieu, L. N., Nguema-Ona, E., Scher, J., & Mbofung, C. (2011). Compositional, spectroscopic and rheological analyses of mucilage isolated from taro (Colocasia esculenta L. Schott) corms. *Journal of Food Science and Technology*, *51*(5), 900-907. https://doi.org/10.1007/s13197-011-0580-0

Pereira, P. R., Corrêa, A. C. N. T., Vericimo, M. A., & Paschoalin, V. M. F. (2018). Tarin, a Potential Immunomodulator and COX-Inhibitor Lectin Found in Taro (Colocasia esculenta). *Comprehensive Reviews in Food Science and Food Safety*, *17*(4), 878-891. https://doi.org/10.1111/1541-4337.12358

Quintero, J., Torres, J. D., Corrales-Garcia, L. L., Ciro, G., Delgado, E., & Rojas, J. (2022). Effect of the Concentration, pH, and Ca^{2+} Ions on the Rheological Properties of Concentrate Proteins from Quinoa, Lentil, and Black Bean. *Foods*, *11*(19), 3116. https://doi.org/10.3390/foods11193116

Schreuders, F. K. G., Sagis, L. M. C., Bodnár, I., Erni, P., Boom, R. M., & van der Goot, A. J. (2021). Small and large oscillatory shear properties of concentrated proteins. *Food Hydrocolloid*s, *110*, 106172. https://doi.org/10.1016/j.foodhyd.2020.106172

Winter, H. H., & Chambon, F. (1986). Analysis of Linear Viscoelasticity of a Crosslinking Polymer at the Gel Point. *Journal of Rheology*, *30*(2), 367-382. https://doi.org/10.1122/1.549853

Zhao, H., Li, W., Qin, F., & Chen, J. (2016). Calcium sulphate-induced soya bean protein tofu-type gels: Influence of denaturation and particle size. *International Journal of Food Science and Technology*, *51*(3), 731-741. https://doi.org/10.1111/ijfs.13010

Zhu, X. F., Zheng, J., Liu, F., Qiu, C. Y., Lin, W. F., & Tang, C. H. (2017). The influence of ionic strength on the characteristics of heat-induced soy protein aggregate nanoparticles and the freeze-thaw stability of the resultant pickering emulsions. *Food & Function*, *8*(8), 2974-2981. https://doi.org/10.1039/c7fo00616k